

## Multiparticle production in $p$ -nucleus and nucleus-nucleus collisions

T. F. Hoang

1749 Oxford Street, Berkeley, California 94709

H. J. Crawford

Space Sciences Laboratory, Lawrence Berkeley Laboratory, Berkeley, California 94720

(Received 22 September 1989)

Kinematic properties of inclusive  $p + A \rightarrow \pi^-$  and  $A_1 + A_2 \rightarrow \pi^-$  at 200 GeV/nucleon are compared with  $p + p \rightarrow \pi^-$  at 200 GeV/c using data of CERN SPS experiments. The partition temperature is found to be practically the same for all the reactions analyzed, suggesting an approximate scaling. The peak shift of pseudorapidity  $\eta$  distributions of these nuclear reactions with respect to the peak of  $pp \rightarrow \pi^-$  follows a geometrical law:  $\eta^* \simeq (A_1^{1/3} - A_2^{1/3})/8$ , independent of energy. The mean free path  $l$  characteristic of the energy loss suffered by the projectile fireball passing through the nuclear target is  $l \simeq 6.21$  fm. Semiempirical formulas for  $\langle n_- \rangle$  of  $p + A$  and  $A_1 + A_2$  reactions are proposed and tested using available data.

### I. INTRODUCTION

Ever since the discovery of large stars in emulsion produced by heavy nuclei of the primary cosmic rays,<sup>1</sup> forty years ago, great interest has been paid to the study of these high-energy nucleus-nucleus reactions. It is a challenge to understand this problem of fundamental importance: How is the prematter created?<sup>2</sup> Recently, experiments of high-energy heavy-ion (HI) reactions at the CERN SPS and BNL AGS-Tandem<sup>3</sup> indicate an abundance of mesons produced in the central region where a phase transition to a quark-gluon plasma is expected to occur according to QCD prediction.<sup>4</sup>

The salient feature of these nuclear reactions is the average  $P_1$  of secondaries from various targets, which is found to be practically the same for the same energy per incident nucleon; see Tables I and II. This suggests that the primary interaction proceeds like  $pp$ : namely, collision of an incident nucleon with a quasi-free nucleon inside the nucleus, followed by secondary collisions with other nucleons of the target.

An attempt is therefore made to analyze the pseudorapidity  $\eta$  distributions of  $p + A \rightarrow \pi^-$  and  $^{16}\text{O} + A \rightarrow \pi^\pm$  at 200 GeV/nucleon of CERN SPS experiments<sup>5-7</sup> as in the case of  $\pi^+p$  and  $K^+p \rightarrow \pi^-$  of a previous work<sup>8(b)</sup> using the Chou-Yang-Yen (CYY) formula,<sup>9</sup> generalized by introducing the shift parameter  $\eta^*$  to account for the asymmetry of the distribution with respect to the axis  $\eta=0$  in the c.m. system (c.m.s.) of the colliding nucleons, Figs. 1 and 2 (Secs. III and IV).

The results of our analysis unravel interesting properties of a geometrical aspect of multiparticle production by high-energy  $p + A$  and HI reactions (Secs. III and IV), especially the behavior of the shift parameter  $\eta^* \sim A^{1/3}$  (Sec. V) and the approximate scaling of the  $\eta$  distribution, Fig. 4, as is expected from the generalized CYY formula (5) (Sec. VI).

The energy loss of the forward fireball (FB) of  $p + A \rightarrow \pi^- + \dots$  passing through the target nucleus of

mass number  $A$  is investigated using the data of  $x$  distributions of an MIT-Fermilab experiment at 100 GeV/c.<sup>10</sup> We find a mean free path (mfp)  $\approx 6.2$  fm comparable to the  $U$  radius (Sec. VII). The energy dissipated in the target nucleus serves to create secondary mesons emitted by the target.

We find practically the same  $T_p^*$  (in the FB system) for  $p + \text{nucleus}$  and  $^{16}\text{O} + \text{nucleus}$  collisions as for  $pp$  at the same GeV/nucleon, Tables I and II, indicating that, in the central region, the energy density is the same for the reactions we have analyzed and that the primary act of interaction is like a nucleon-nucleon collision followed by secondary interactions in the nuclear target. This mechanism leads to a semiempirical formula for the ratio of negative multiplicities of  $pA$  to  $pp$ , Eq. (16), in good agreement with experimental values from  $P_{\text{lab}} = 9.9-360$  GeV/c (Sec. VIII). The formula is extended to the HI reactions, Eq. (18), and charged multiplicity, Eq. (19).

Some remarks will be made (Sec. IX) on the geometrical properties of multiparticle production by nuclear reactions, especially the application of the Chou-Yang-Yen formula, Eq. (5), which enables us to get some insight into this complex problem of high-energy HI reactions.

### II. THE PARTITION-TEMPERATURE MODEL

In an attempt to investigate the kinematic properties of multiparticle production by high-energy nuclear reactions of CERN-SPS experiments (see below) we are led to analyze the c.m. pseudorapidity  $\eta = -\ln(\tan\theta/2)$  distributions (Figs. 1 and 2) in the context of the partition-temperature  $T_p$  model of Chou, Yang, and Yen<sup>9</sup> (CYY). Consider first the case of inclusive

$$p + p \rightarrow \pi^- + \dots,$$

as has been reported previously;<sup>8(a)</sup> we may use the CYY formula for the  $\eta$  distribution of zero mass particles in the c.m.s. of collision,

$$\frac{dn}{d\eta} = \frac{N}{\left[ \alpha + \frac{1}{T_p} \cosh \eta \right]^2}, \quad (1)$$

where  $\alpha = 2/\langle P_{\perp} \rangle$  is a fixed parameter corresponding to an exponential cutoff on the transverse momentum,  $T_p$  the partition temperature, and  $N$  the normalization coefficient.

Note that in the case of fixed-target experiments, the passage from the laboratory system to the c.m.s. is straightforward:

$$\eta_{\text{lab}} = \eta + \eta_{\text{c.m.}}, \quad (2)$$

where  $\eta = \ln(\cot \theta_{\text{c.m.}}/2)$  is the pseudorapidity of a secondary in the c.m.s. of colliding  $pp$  and  $\eta_{\text{c.m.}}$  is that of the  $pp$  c.m.s. with respect to the laboratory system, namely,

$$\eta_{\text{c.m.}} = \frac{1}{2} \ln \frac{1 + \beta_{\text{c.m.}}}{1 - \beta_{\text{c.m.}}} \simeq \frac{1}{2} \ln \frac{2P_{\text{lab}}}{m_p}, \quad (3)$$

$\beta_{\text{c.m.}}$  being the velocity of the  $pp$  c.m.s. in the laboratory system.

We recall that  $T_p$  in Eq. (1) represents the average energy of produced secondaries in their *rest frame*, referred to as the *initial* fireball (FB), which subsequently splits into two: one forward (FD) and another backward (BD), associated with the colliding protons. Clearly, these two FB's are symmetric just as the system  $pp$  in the initial state, so that their c.m.s. coincides with the c.m.s. of the colliding  $pp$ .

As regards  $p + A \rightarrow \pi^-$ , there are more  $\pi^-$ 's in the BD direction than in the FD, as is seen from Fig. 1. Note that the asymmetry is still more striking in the case of HI reactions  $^{16}\text{O} + A$  as is shown in Fig. 2.

Therefore, to apply the CY formula (1) to the asymmetric  $\eta$  distributions we are dealing with, we have to use an appropriate frame, namely, the *initial* FB rest frame before its breakup into FD and BD ones associated with the projectile proton and the target nucleus, disregarding the c.m.s. of the primary collision of the incident nucleon with a nucleon of the target nucleus, and that of other  $\pi^-$ 's from secondary reactions inside the target nucleus. For this purpose, we replace, in (1)

$$\eta \rightarrow \eta - \eta^* \quad (4)$$

and write

$$\frac{dn}{d\eta} = \frac{N}{\left[ \alpha + \frac{1}{T_p^*} \cosh(\eta - \eta^*) \right]^2}, \quad (5)$$

where the asterisk is to specify the rest frame of the *initial* FB in which the partition temperature should be estimated. Note that  $\alpha$  is invariant like  $\langle P_{\perp} \rangle$  (see above). Kinematical considerations indicate that  $\eta^*$  is determined by the rapidities  $\eta_{\text{FB}}^*$  and  $\eta_{\text{BD}}^*$  ( $< 0$ ) of the FD and BD fireballs (see below):

$$\eta^* = \eta_{\text{FD}}^* + \eta_{\text{BD}}^*, \quad (6)$$

which has been discussed and verified in Ref. 8(b). Note that  $\eta^* = 0$ , if  $\eta_{\text{FD}}^* = |\eta_{\text{BD}}^*|$ , i.e., the FD and the BD FB's are symmetric.

As regards the kinematics of the FB, we note, in passing, that its velocity  $\beta^*$  may be estimated by using the covariant Boltzmann factor as follows:

$$f \approx e^{-(E - \beta^* P_{\parallel})/T}, \quad (7)$$

where  $(E, \mathbf{P})$  are the energy and the momentum in c.m.s. of a secondary particle of  $p + A \rightarrow \pi^-$ , in one hemisphere and  $T$  the conventional temperature determined by  $\langle P_{\perp} \rangle$  (see, e.g., Ref. 4). As reported previously,<sup>11,12</sup>  $\beta^*$  may be estimated independently of  $T$  by using the c.m.s. angular distribution; or else we may use the distribution of  $x = 2P_{\parallel}/\sqrt{s}$ , namely,

$$\frac{dn}{dx} \sim x e^{-ax} \quad (8)$$

according to (7), with

$$a \equiv (1 - \beta^*)\sqrt{s}/2T. \quad (9)$$

Finally, we mention that the Boltzmann factor (7) resembles that used by Fermi for the angular momentum conservation of secondary particles, and that it was originally introduced to describe the Feynman-Yang scaling,<sup>13</sup> whereas Li and Young use the factor (7) for their partition-temperature model of  $p$ -nucleus reactions<sup>14</sup> in a different context, namely, the microcanonical ensemble approach.

### III. INCLUSIVE $p + A \rightarrow \pi^-$ REACTIONS

We now proceed to analyze the data of  $p + A \rightarrow \pi^-$  at 200 GeV/c of the NA5 Collaboration<sup>5</sup> and the NA35 Collaboration.<sup>6</sup> Their measurements of  $\langle n_- \rangle$  and  $\langle P_{\perp} \rangle$  (in MeV/c) are summarized in Table I. It is interesting to note that  $\langle P_{\perp} \rangle$  is practically the same for  $p + A \rightarrow \pi^-$  as for  $p + p \rightarrow \pi^-$ , suggesting that the primary interaction of  $p$ -nucleus reaction takes place with a single nucleon of the target, the Fermi motion being negligible.

TABLE I. Parameters of inclusive  $p + A \rightarrow \pi^-$  at  $P_{\text{lab}} = 200$  GeV/c,  $\eta_{\text{c.m.}} = 3.02$ , NA5 Collaboration, Ref. 5.

	$pp$	$p\text{Ar}$	$p\text{Xe}$
$\langle n_- \rangle$	$2.96 \pm 0.03$	$5.39 \pm 0.17$	$6.89 \pm 0.13$
$\langle P_{\perp} \rangle$ (MeV/c)	$366 \pm 2$	$376 \pm 3$	$363 \pm 3$
$\eta^*$	$\equiv 0$	$-0.46 \pm 0.03$	$-0.66 \pm 0.01$
$T_p^*$ (GeV)	$0.547 \pm 0.049$	$0.816 \pm 0.137$	$0.642 \pm 0.062$
$N$	$45.5 \pm 10.4$	$62.4 \pm 8.5$	$75.9 \pm 11.2$

With this remark, we assume  $y=\eta$  and find from (3)  $\eta_{c.m.}=3.03$ . The  $\eta$  distributions in the c.m.s. of the incident  $p$  and a nucleon of the target  $A$  are shown in Fig. 1. The asymmetry is conspicuous by referring to the line at  $\eta=0$ , namely, the  $F/B$  ratio of  $\pi^-$  is  $<1$ : compared to  $1.04\pm 0.02$  for  $p+p\rightarrow\pi^-$  of the same experiment, which is symmetric, according to parity conservation of strong interactions.

As we do not have the  $x$  distributions of these reactions, we are unable to determine  $\eta^*$  using (6). We therefore use the CYY formula (5) to fit the data leaving both  $\eta^*$  and  $T_p^*$  as free parameters, whereas  $\alpha$  is computed using the values of  $\langle P_\perp \rangle$  in Table I, the fit range being  $\eta=\pm 3.0$ . The estimates of  $T_p^*$  (GeV) and  $\eta^*$  thus obtained are listed in Table I.

Note that for  $p+p\rightarrow\pi^-$ ,  $\eta^*=0.022\pm 0.006$  consistent with zero as should be for symmetric distributions. We therefore set it equal to zero. The shifts  $\eta^*$  for  $pAr$  and  $pXe$  are shown by the dotted-dash segments in Fig. 1.

A comparison with the data indicates that the fits are satisfactory, especially in the region around the peak. Here, we find the seagull effect attenuated, in contrast with the case of  $h^+p\rightarrow\pi^-$  of a previous work.<sup>8(a)</sup> This justifies *a posteriori* the assumption of a constant  $\alpha=2/\langle P_\perp \rangle$ .

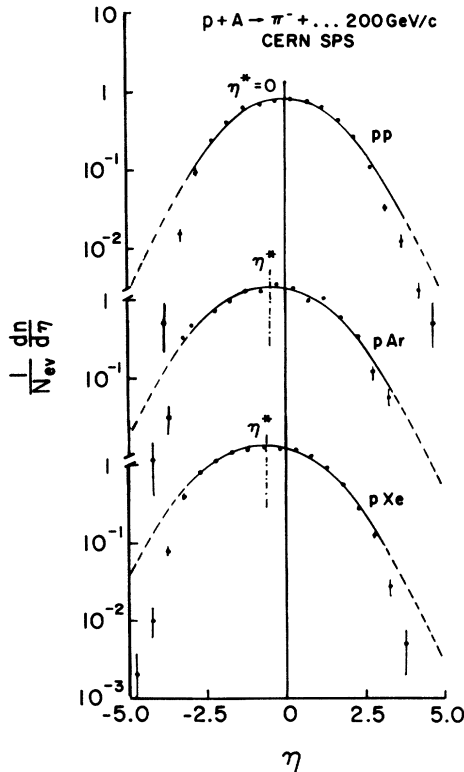


FIG. 1. Pseudorapidity distributions of inclusive  $p + A \rightarrow \pi^-$  at  $P_{lab}=200$  GeV/c. The peak shift  $\eta^*$  with respect to the c.m.s. is characteristic of the asymmetry of the projectile and the target fireballs. The curves are fits using the generalized CYY formula Eq. (5), for  $-3.0 < \eta < +3.0$ , the dotted lines are extrapolations. Parameters are in Table I. The shift parameters  $\eta^*$  are shown by the dotted-dashed lines.

The partition temperatures of  $p$ -nucleus reactions are comparable to that of  $pp$ , within large errors, as in the case of  $T$  determined by  $\langle P_\perp \rangle$  as is listed in Table I (see Ref. 15). For the parameter  $\eta^*$  which describes the asymmetry of the FB's associated with the projectile proton and the target nucleus, Eq. (6), it increases with the size of the target, its  $A$  dependence will be investigated later on, together with the nucleus-nucleus reactions (Sec. VI).

In addition to these distributions we have also analyzed the  $\eta$  distribution of *charged secondaries* of  $p+Xe$ . We find  $\eta^*=0.52\pm 0.03$  and  $T_p^*=0.911\pm 0.085$  GeV, indicating the same shift in the peak of the distribution, whereas  $T_p^*$  is somewhat greater than that of  $p+Xe\rightarrow\pi^-$ , as is listed in Table I. This difference may be caused by the mixture of nuclear particles of the target evaporation (see Sec. IX).

Finally, we have investigated the  $\pi^-$  absorption by the nuclear targets Ar and Xe, but no perceptible effect has been found for the NA5 data. A discussion of this investigation is given in the Appendix, as regards the slight asymmetry of their  $\eta$  distributions in Fig. 1 with respect to the axis at  $\eta^*$ . This may be due to the Coulomb scattering which is different for  $\pi^-$ 's from the fragmentations of the proton projectile and the nucleus target. On the other hand, we recall that the asymmetry around the peak has been found to increase with the number of collisions suffered by the incident proton inside the nucleus target.<sup>16,17</sup> Nonetheless, if we compare the asymmetry of each  $\eta$  distribution in Fig. 1 with respect to the  $\eta^*$  axis, we find that it is imperceptible for  $|\eta| < 2.2$ , amounting to  $\sim 80\%$  of the data, indicating that it will not affect our parametrization.

#### IV. HI REACTIONS $^{16}O + A \rightarrow h^\pm$

We turn next to the CERN-SPS experiments  $^{16}O + A$  at 200 GeV/nucleon of the WA80 Collaboration.<sup>7</sup> As is well known, the multiplicities of these high-energy HI reactions are extremely high; the ratios of  $\langle n_- \rangle$  for HI reaction to  $p$  nucleus of the same  $A$  at  $P_{lab}=200$  GeV/c are listed in Table III (bottom). But, in spite of the large number of secondaries emitted in these HI reactions, the average transverse momentum of  $\sim 350$  MeV/c remains almost the same as  $\langle P_\perp \rangle$  of  $p$  nucleus and  $pp$  reactions at  $P_{lab}=200$  GeV/c (see Table I). This indicates that the secondaries observed in the final state of a HI reaction result from a *superposition* of primary interactions, each of which is a nucleon-nucleon collision, one from the projectile and another from the target, their Fermi motions being negligible.

We are therefore led to analyze the  $\eta$  distributions of the WA80 Collaboration<sup>7(a)</sup> (in laboratory system), reproduced in Fig. 2, error bars being hidden by the data points. For convenience, as in the previous case of  $p + A$ , we set  $\eta_{c.m.}=3.03$  and  $\alpha=5.41$ . The parameters thus obtained are summarized in Table II. The fits are shown in Fig. 2. They are very satisfactory, indeed. Here again, we find little seagull effect as in the case of inclusive  $p + A$  reactions discussed in the preceding section.

TABLE II. Parameters of inclusive  $^{16}\text{O} + A \rightarrow h^\pm$  at 200 GeV/nucleon,  $\eta_{c.m.} = 3.02$ , WA80 Collaboration, Ref. 7.

	Au	Ag	Cu	C
$\langle P_\perp \rangle$ (MeV/c)	$\sim 350$	$\sim 350$	$\sim 350$	$\sim 350$
$\eta^*$	$-0.44 \pm 0.05$	$-0.25 \pm 0.02$	$-0.13 \pm 0.02$	$+0.12 \pm 0.03$
$T_p^*$ (GeV)	$0.831 \pm 0.076$	$0.764 \pm 0.099$	$0.498 \pm 0.024$	$0.870 \pm 0.086$
$N$	$292 \pm 52$	$234 \pm 60$	$235 \pm 91$	$630 \pm 42$

We find  $T_p^*$  comparable to those of  $p + A$  and  $pp$  as is expected from the fact that the temperature for these heavy-ion reactions,  $T \sim 142$  MeV,<sup>6(a)</sup> corresponding to  $\langle P_\perp \rangle \approx 350$  MeV/c is comparable to those of  $p + A$  and  $pp$  listed in Table I. Therefore, the average energy density in the central region is about the same for all nuclear reactions,  $p + A$  and  $A_1 + A_2$  alike, as for  $pp$  at the same incident energy/nucleon.

Consider next the parameter  $\eta^*$  in Table II. We note that the magnitude of  $\eta^*$  increases monotonically with the nuclear size  $A$  of the target, Fig. 3, indicating that the maximum of the  $\eta$  distribution, according to (6), shifts backward or forward according to the relative size of the target compared to the projectile. Note especially that  $\eta^*$  of the C target is positive.

Finally, it should be mentioned that the backward shift of maximum has been reported by the authors of the WA80 Collaboration<sup>7</sup> and it has also been reported that "new phenomenon cannot be excluded." It is therefore expedient to investigate the properties of this parameter  $\eta^*$  we have used to generalize the CYY formula (1) to account for the asymmetry of FB's associated with the projectile and the target.

### V. THE $A$ DEPENDENCE OF $\eta^*$

As has been mentioned before (Secs. I and II), the shift  $\eta^*$  of the maximum of the  $\eta$  distribution is essentially a

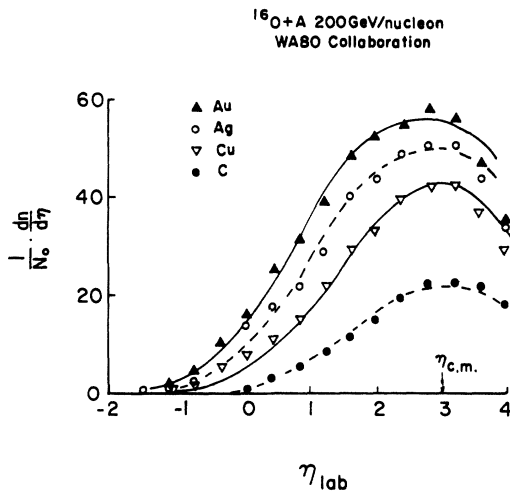


FIG. 2. Pseudorapidity distributions of  $A_1 + A_2 \rightarrow h^\pm$  at 200 GeV/A. WA80 experiment, Ref. 7. Note the increase of the peak shift  $\eta^*$  with  $A$ . The curves represent the  $T_p$  model fits. Parameters are listed in Table II.

kinematic effect. It reflects the asymmetry of the FB's associated with the projectile  $A_1$  and the target  $A_2$ , just as in the case of inclusive  $\pi^+ p \rightarrow \pi^-$  or  $K^+ p \rightarrow \pi^-$  discussed elsewhere.<sup>8(b)</sup> Since the FB's move along the collision axis, in the opposite directions, we expect the effect of  $\eta^*$  to be a function of the linear dimensions of the projectile  $A_1$  and the target  $A_2$ .

Indeed, the  $A_2^{1/3}$  dependence of  $\eta^*$  is self-evident from the point of view of the effective  $E_{lab}$  of the projectile, which decreases as it passes inside the nucleus (see Sec. VII). This is shown by the plot of  $\eta^*$  values of  $p + A$  and  $^{16}\text{O} + A$  listed in Tables I and II. Remembering that  $\eta^* = 0$  for symmetric FB's, i.e., collision of like particles,  $A_1 = A_2$ , we therefore write

$$\eta^* = c(A_1^{1/3} - A_2^{1/3}) \quad (10)$$

and find, by the least-squares fit for  $p + A$  and  $^{16}\text{O} + A$  analyzed in Secs. III and IV (the  $pp$  case being included as a constraint of the fit),

$$c = 0.127 \pm 0.020.$$

The fit is good, except for the deviation of the  $p + A$  point. This may well be due to statistics: i.e., the NA5 experiment disposes of 2000 pictures for  $pAr$  amounting to  $\frac{1}{2}$  the number of  $pXe$  pictures, which have a larger cross section.

Next, an attempt is made to investigate the energy dependence of  $\eta^*$ . For this purpose, we tentatively make

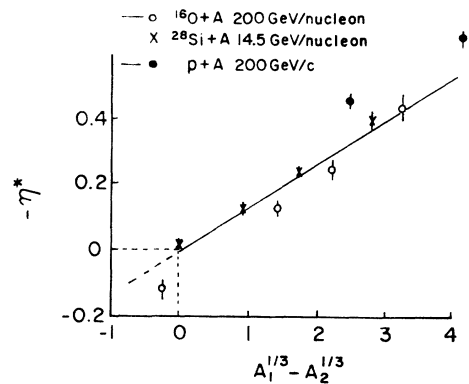


FIG. 3. Behavior of the peak-shift parameter  $\eta^*$ . The values of  $\eta^*$  for  $pA$  (solid circles) and  $A_1 + A_2$  (open circles) reactions in Tables I and II are plotted vs the difference in nuclear size. The straight line is the least-squares fit to these two sets of data. The crosses, not included in the fit, are from a BNL experiment at 14.5 GeV/nucleon, Ref. 11, indicating energy independence of  $\eta^*$ .

use of the preliminary data of BNL experiment E802,  $^{28}\text{Si} + A$  at 14.5 GeV/nucleon using Al, Cu, Ag, and Au targets.<sup>18</sup> The  $\eta^*$ 's are shown in Fig. 3 by crosses, they fall perfectly on the fitted straight line for the CERN-SPS experiments; to the point that if we do the same fit for the BNL points only, we then get

$$c = 0.128 \pm 0.007$$

in excellent accord with the previous fit for the CERN-SPS data.

It is worth noting that the size of the  $^{27}\text{Al}$  target is very close to that of the  $^{28}\text{Si}$  beam. We find from their data  $\eta^* = 0.04 \pm 0.02$  consistent with zero, suggesting that  $\eta^*$  changes sign according to the relative size of the projectile and the target.

This remarkable property of geometrical aspect of the  $\eta^*$  parameter is a characteristic feature of particle production in the central region of nuclear reactions. The authors of WA80 find all *backward* (in their notation) shifts of maximum, independent of the mass number of the target.

## VI. SCALING OF THE $\eta$ DISTRIBUTION

We continue to investigate the behavior of  $T_p^*$  of HI reactions in Table II. Apart from the case of Cu, the values of  $T_p^*$  for C, Ag, and Au are practically the same within large statistical errors<sup>15</sup> and  $1/T_p^* < \alpha$  which is practically the same for all the reactions under consideration as  $\langle P_1 \rangle$ .

Consequently, the  $\eta$  distributions in Fig. 2 may be superimposed into one pattern, if we slide each distribution by  $-\eta^*$  and divide it by the normalization coefficient of (5), as is expected from the generalized CYY formula (5).

Figure 4 shows the plots of  $(1/N_\sigma)dn/d\eta$ , i.e., percentage of secondaries vs  $\eta_{\text{lab}} + \eta^*$  of  $^{16}\text{O} + A$  of the WA80 Collaboration where  $\eta_{\text{lab}} = \eta + 3.03$  and  $\eta^*$  is the shift relative to the target  $A$ .<sup>7</sup> We see the scaling property for Cu, Ag, and Au, whereas the carbon data deviates systematically from this property, especially in the target re-

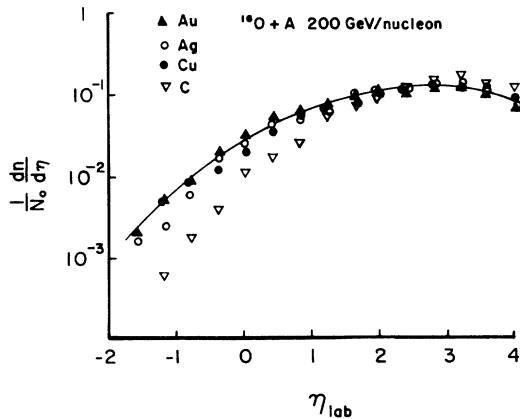


FIG. 4. Plots of shifted  $\eta$  distributions (in percentage) of  $^{16}\text{O} + A$  vs  $\eta - \eta^*$ . The curve shows the property required by the Chou-Yang-Yen formula, Eq. (5), see text.

gion. We shall leave aside the C data in the following analysis.

If we try an overall fit to the Cu, Ag, and Au data in Fig. 4 using the CYY formula and assuming the same  $\alpha = 5.41$  as before (Sec. IV), we find

$$\bar{T}_p^* = 0.93 \pm 0.04 \text{ GeV}, \quad \bar{N} = 132.5 \pm 14.8.$$

The fit is shown by the solid curve in Fig. 4, in satisfactory agreement with the data of Cu, Ag, and Au.

It should be mentioned that both the partition temperature  $\bar{T}_p^*$  and the normalization coefficient  $\bar{N}$  thus obtained are significantly higher than the estimates of  $T_p^*$  of individual fits in Table II, indicating that the scaling we are dealing with is only approximate. Note that a crucial test of this important property needs especially data of FD secondaries, namely, from the projectile fragmentation, which are expected to be independent of  $A$ , so that they are independent of  $\eta^*$ , according to the limiting fragmentation.

Finally it should be mentioned that the scaling here discussed is different from that of Nakamura and Kudo.<sup>16</sup> Their approach is based on the well-known Kobayashi-Nielsen-Olesen scaling for the multiparticle production of inclusive reactions: namely, they plot against  $\eta/\langle \eta \rangle$ .

## VII. PASSAGE OF THE PROJECTILE FB THROUGH A NUCLEAR TARGET

When the projectile FB of  $p + A \rightarrow \pi^-$  passes through the target  $A$ , it interacts with the nuclear stuff, i.e., nucleons, mesons, etc., so it slows down and loses energy. The energy thus dissipated is used for secondary production inside the target. We therefore have to compute the velocity  $\beta^*$  of the projectile FB (in the c.m.s. of collision), or its Lorentz factor  $\gamma_F = 1/\sqrt{1-\beta^{*2}}$ .

We recall that the FB at the initial stage of the reaction is that of  $p + p \rightarrow \pi^-$  at the same energy  $\sqrt{s}$  and that  $\beta^*$  is given by the scaling property discussed previously,<sup>12</sup> namely,  $\beta^* = 1 - 2/\gamma_{\text{c.m.}}$  with  $\gamma_{\text{c.m.}} = \sqrt{s}/2m_p$ .

After its passage through the nuclear target, we have to estimate  $\beta^*$  using the forward  $x$  distribution of  $p + A \rightarrow \pi^-$  by the formulas (8) and (9) to compute  $\gamma_F$ . As we do not have the  $x$  distributions of the CERN-SPS experiments we are dealing with in the present work, we will use the data of Fermilab experiment E116,  $p + A \rightarrow \pi^-$  at 100 GeV/c of the MIT-Fermilab Collaboration,<sup>10</sup> with  $p$ , C, Cu, and Pb targets. We analyze their data of  $Ed\sigma/dp^*$  at  $P_1 = 0.3$  GeV/c, using (8) and assuming  $T = 139$  MeV to estimate  $\beta^*$  and  $\gamma_F$ . The results thus obtained are plotted in Fig. 4 versus the specific effective radius  $R/r$  where  $R = \sqrt{\sigma_{\text{inc}}/\pi}$  and  $r$  is the nuclear radius parameter.

We recall that, according to the optical model,<sup>19(a)</sup>

$$R(A) = r \left[ A^{1/3} - \frac{a}{A^{1/3}} \right], \quad (11)$$

account being taken of the absorption by the second term:

$$a = (\lambda/2r)^2, \quad (12)$$

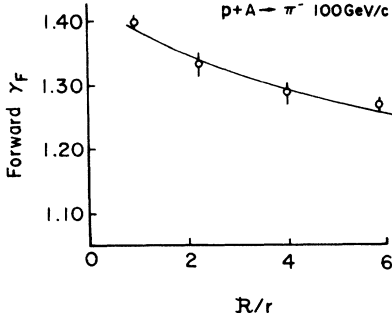


FIG. 5. Energy loss of the projectile fireball (FB) passing through a nuclear target,  $p + A \rightarrow \pi^- + \dots$  at 100 GeV/c. Data from the MIT-Fermilab experiment, Ref. 10. The plot represents the Lorentz factor of the FB vs the effective nuclear radius of the target, see text. The curve represents an exponential fit with a mean free path  $l = 6.21 \pm 0.03$  fm.

$\lambda$  being the absorption mean free path. From a previous analysis of  $pA$  reactions at  $P_{\text{lab}} = 10-100$  GeV/c, we get, for the parameters<sup>19</sup> (in fm),

$$r = 1.30 \pm 0.01, \quad \lambda = 1.44 \pm 0.23.$$

It is worth noting that  $\lambda \approx 1/m_{\pi}$ .

If we describe the behavior of  $\gamma_F$  of the projectile FB by an exponential law with a characteristic mean free path  $l$ , namely,

$$\gamma_F \sim \exp(-R/l\gamma_{\text{c.m.}}), \quad (13)$$

where  $\gamma_{\text{c.m.}} = 7.37$  is the Lorentz contraction factor. We find

$$l = 6.21 \pm 0.03 \text{ fm}.$$

The fit shown by the curve in Fig. 5 is satisfactory.

It is interesting to note that this mean free path is quite comparable to the U radius, but somewhat between 4.9 and  $8 \pm 2$  fm estimated by Csernai *et al.*<sup>20(a)</sup> and by Daté *et al.*<sup>20(b)</sup> for the mean degradation length of the proton of inclusive  $p + A \rightarrow p + \dots$  at 100 GeV/c of the same MIT-Fermilab experiment,<sup>10</sup> as analyzed here.

### VIII. THE MULTIPLICITY

As is well known, the property of limiting fragmentation holds for  $p + A \rightarrow \pi^-$  as is reported by the MIT-Fermilab experiment.<sup>10</sup> Therefore, we may separate its multiplicity into forward (FD) and backward (BD) parts corresponding to the fragmentations of the projectile  $p$  and the target nucleus  $A$ , respectively:

$$\langle n_- \rangle_{pA} = \langle n_- \rangle_p + \langle n_- \rangle_A \quad (14)$$

with

$$\langle n_- \rangle_p = \frac{1}{2} \langle n_- \rangle_{pp} \quad (15)$$

at the same energy, which can be predicted accurately using the scaling property of inclusive  $p + p \rightarrow \pi^-$ .<sup>19(b)</sup>

As regards  $\langle n_- \rangle_A$ , in addition to the mesons pro-

TABLE III. *Top part:* Comparison between experimental ratios  $\langle n_- \rangle_{pA} / \langle n_- \rangle_{pp}$  and predictions by  $R(A) = \frac{1}{2}(1 + A^{\alpha/3})$ , Eq. (16) with  $\alpha = 0.80$  according to NA5 data at  $P_{\text{lab}} = 200$  GeV/c. *Bottom part:* Comparison of the negative multiplicity of  $^{16}\text{O} + A$  at 200 GeV/nucleon  $R(A_1 A_2) = \langle n_- \rangle_{A_1 A_2} / \langle n_- \rangle_{pA_2}$  with the prediction Eq. (18), see text.  $O$  denotes the equivalent  $A$  of the mixture 20% He and 80% Ne of the steamer chamber.

$P_{\text{lab}}$ (GeV/c)	Target $A$	Ratio $\langle n_- \rangle_{pA} / \langle n_- \rangle_{pp}$	
		Experimental	Prediction
200	$p$	1.00	1.00
	$^{40}\text{Ar}$	$1.83 \pm 0.08$	1.80
	$^{132}\text{Xe}$	$2.33 \pm 0.04$	2.32
9.9	$^{12}\text{C}$	$1.52 \pm 0.09$	1.47
28	$^{20}\text{Ne}$	$1.70 \pm 0.13$	1.56
360	$^{197}\text{Au}$	$2.76 \pm 0.10$	2.56
		Ratio $\langle n_- \rangle_{A_1 A_2} / \langle n_- \rangle_{pA_2}$	
	Target $A_2$	Experimental	Prediction
	$^{15.7}\text{O}$	$5.85 \pm 0.24$	5.80
	$^{64}\text{Cu}$	$11.7 \pm 0.6$	11.7
	$^{197}\text{Au}$	$15.4 \pm 0.5$	15.2

duced in the primary interaction of one of its constituent nucleons with the incident  $p$ , there are also secondary mesons arising from the energy loss of the projectile FB and rescattering of particles inside the target nucleus. We may, for simplicity, describe these secondary processes in terms of an empirical power law  $A^\alpha$ , which is, to some extent, equivalent to the Glauber theory.<sup>21</sup> Therefore, we propose to describe the  $A$  dependence of  $\langle n_- \rangle_{pA}$  by a semiempirical formula as follows, in the form of a ratio to  $\langle n_- \rangle_{pp}$  at the same energy:

$$R(A) = \langle n_- \rangle_{pA} / \langle n_- \rangle_{pp} = \frac{1}{2}(1 + A^{\alpha/3}), \quad (16)$$

where we have expressed explicitly the target dimension  $A^{1/3}$ , a property of the geometric aspect discussed above. The parameter  $\alpha$  to be estimated using the experimental data is expected to be  $\sim 1$ . Note that (16) may be derived from the multiple collision model by keeping only the leading term corresponding to one collision.

We use the negative multiplicity from  $p + A \rightarrow \pi^- + \dots$  at 200 GeV/c listed in Table I to estimate the parameter  $\alpha$ ; with the  $pp$  case serving as a constraint, namely,  $R(1) \equiv 1$ . We get

$$\alpha = 0.80 \pm 0.16$$

The predicted multiplicities, Table III (top), agree rather well with the experimental ratios.

As a consistency check of our parametrization, we have used other available data of  $p + A \rightarrow \pi^-$ , with different targets and at different energies, from  $P_{\text{lab}} = 9.9-360$  GeV/c.<sup>22</sup> The predictions by (16) are in Table III (top). The agreement is satisfactory, indicating that  $\alpha$  is likely not sensitive to the energy and that  $\alpha \neq 1$  by  $\sim 1$  standard deviation (s.d.) is probably due to some screening effect in the rescattering process.

As regards the multiplicities of HI reactions, we may

extend (16) for  $p + A \rightarrow \pi^-$  to nucleus-nucleus reactions:  $A_1 + A_2 \rightarrow \pi^-$ . We make use of this property of their cross sections according to the optical model, reported previously,<sup>19(a)</sup>

$$A^{1/3} \rightarrow A_1^{1/3} + A_2^{1/3} \quad (17)$$

and assume the large- $A$  approximation to get, as in the case of (16),

$$\begin{aligned} R(A_1, A_2) &= \langle n_- \rangle_{A_1, A_2} / \langle n_- \rangle_{p, A_2} \\ &= C[1 + (A_1^{1/3} + A_2^{1/3})^\beta], \end{aligned} \quad (18)$$

where  $\beta$  is a parameter to be compared with  $\alpha$  of (16) and  $C$  a coefficient such that  $R(1,1)=1$  as a consistency check (see below).

We use the data of a streamer-chamber experiment  $^{16}\text{O} + A \rightarrow \pi^- + \dots$  at 200 GeV/ $A$  by the NA35 Collaboration.<sup>6</sup> The experimental ratios  $R(A_1, A_2)$  are listed in Table III (bottom), the values of  $\langle n_- \rangle_{p, A_2}$  being computed by (16). Note that the effective mass number of the mixture 20% He and 80% Ne is 15.7 close to that of the oxygen projectile; we find

$$\beta = 1.91 \pm 0.18, \quad C = 0.26 \pm 0.02.$$

The computed ratios are listed in Table III (bottom), in excellent agreement with the experimental values. As a consistency check of our parametrization, we have computed the ratio (18) for  $A_1 = A_2 = 1$  and found  $R(1,1) = 1.24 \pm 0.26$  consistent with  $R(1,1) = 1$  according to the definition (18). Next, we note that  $C = 0.26$  is about  $\frac{1}{2}$  of the corresponding coefficient in (16) for  $p + A \rightarrow \pi^-$ . This is expected from the symmetry of  $R_{12}/r = A_1^{1/3} + A_2^{1/3}$ ; more specifically, (18) remains the same for the reversed reaction  $A_1 \rightleftharpoons A_2$ . The HI reactions we are dealing with are fixed-target experiments, the reversed reactions being unaccounted for. In this regard, we have to bear in mind that the c.m.s. energy  $\sqrt{s}$  may be different for the reversed reaction so that the direct and the reversed HI reactions may not be treated on equal footing.

As regards the charged multiplicity, we find that it may be expressed in terms of  $\langle n_- \rangle$  by means of the charges  $Z_1$  and  $Z_2$  of the projectile and the target as

$$\langle n_{\text{ch}} \rangle = \langle n_- \rangle \frac{A_1 + A_2}{Z_1 + Z_2}. \quad (19)$$

Note that (19) holds also for the  $p$ -nucleus reactions of NA35 Collaboration<sup>6</sup> discussed above.

Finally, we note that

$$\beta \simeq 2\alpha, \quad (20)$$

suggesting that the pion production by HI reactions is a surface emission rather than a bremsstrahlung around the collision axis as in the case of  $p + A \rightarrow \pi^-$  with  $\alpha \simeq 1$  as expected from Landau's model.

## IX. CONCLUDING REMARKS

The results of our analysis of the  $\eta$  distributions of  $p$ -nucleus and HI reactions of CERN-SPS experiments at

the same energy 200 GeV/nucleon<sup>5-7</sup> using formula (5) of the partition-temperature  $T_p$  model of Chou, Yang, and Yen<sup>9</sup> indicate that  $T_p^*$  in the FB system is practically the same as for the  $p + p \rightarrow \pi^-$  at  $P_{\text{lab}} = 200$  GeV/ $c$ . The fits, Figs. 1 and 2, are excellent, especially for the HI reactions, compared to the fits presented by the authors of the NA80 Collaboration using the Fritiof model.<sup>7(a)</sup>

We have introduced the shift  $\eta^*$ , Eq. (4), to describe the asymmetry of the FB's in nuclear reactions, in analogy with  $\pi^+ p \rightarrow \pi^-$  compared to  $pp \rightarrow \pi^-$  reported previously.<sup>8(b)</sup> This parameter describes the *peak shift* of  $\eta$  distributions observed by the WA80 Collaboration, but "not understood."<sup>6(a)</sup> We find that  $\eta^*$  has this simple and remarkable property of geometrical aspect, namely,  $\eta^* \sim A^{1/3}$  and independent of energy Fig. 3. However, no such peak shift has been observed in emulsion data.<sup>23</sup> This may be due to the systematics of using the shower tracks with  $\beta > 0.7$  and the mixture of nuclear particles from Br and Ag targets. It is not known how these causes may affect the shape of the  $\eta$  distribution near the maximum.

The salient feature of the  $\eta$  distributions of  $p$ -nucleus and HI reactions, Figs. 1 and 2, analyzed in the present work is that  $T_p^*$  is comparable within large errors. Consequently, according to the generalized CY formula (5), the  $\eta$  distributions have the scaling property (Sec. VI). However, we find it valid only for HI reactions with large targets, at variance with the scaling proposed by Nakamura and Kudo.<sup>16</sup>

We find different  $A$  dependence for  $\langle n_- \rangle$  of  $p + A \rightarrow \pi^-$  and  $^{16}\text{O} + A \rightarrow \pi^-$  Eqs. (16) and (18), reflecting to some extent, different mechanisms of multiparticle production. These semiempirical formulas, based on general grounds of kinematical considerations, may be useful to test various models proposed for the multiparticle production by nuclear reactions.

## ACKNOWLEDGMENTS

The authors wish to thank G. Gidal and I. Hinchliffe for many discussions and comments. One of the authors (T.F.H.) renews acknowledgment to Professor L. Leprince-Ringuet for having guided him with enduring inspiration to study reactions initiated by heavy nuclei of cosmic rays; he would like to thank L. Wagner for facilitating the work at Lawrence Berkeley Laboratory and the Tsi Jung Fund for the support. This work was supported by the Director, Office of Energy Research, Division of Nuclear Physics, Office of High Energy and Nuclear Physics, of the U.S. Department of Energy under Contract No. DE-AC03-76SF00098, and by NASA under Grant No. NGR05-003-513.

## APPENDIX

We have made a crude estimation of the absorption cross section  $\sigma$  of  $\pi^-$ -nucleus reactions using the optical model

$$\sigma = \pi \int_{0 \leq b \leq R} (1 - e^{-2x\lambda}) db^2, \quad (A1)$$

where  $b$  is the impact parameter,  $x = \sqrt{R^2 - b^2}$  the

traversal,  $R = rA^{1/3}$  being the nuclear radius, and  $\lambda$  the absorption mean free path (mfp):

$$\lambda = 1/\rho_0 \bar{\sigma}_{\pi N}, \quad (\text{A2})$$

$\rho_0 = 0.17$  nucleon  $\text{fm}^{-3}$  being the nuclear density and  $\bar{\sigma}_{\pi N} = (\sigma_{\pi+p} + \sigma_{\pi-p})/2$  the average total  $\pi$ -nucleon cross section. We use large  $A$  approximation after integration of (A1) to get<sup>24</sup>

$$\sigma = \pi r^2 \left[ A^{1/3} - \frac{(\lambda/2r)^2}{A^{1/3}} \right]^2. \quad (\text{A3})$$

We have used the currently available experimental data of  $\pi^\pm A$  absorption cross sections<sup>25</sup> and those of phase-shift analyses by Höhler *et al.*<sup>26</sup> to estimate the radius parameter  $r$  and the mfp from  $P_{\text{lab}} = 0.1 - 10$  GeV/c, some values (in fm) are shown in Fig. 6. Both parameters  $r$  and  $\lambda$  remain practically constant at higher energies,  $P_{\text{lab}} > 10$  GeV/c, as has been noted in a previous report.<sup>27</sup>

In an attempt to estimate the effect of nuclear absorption of  $\pi^-$  by the target in our analysis of the NA5 experiment we have computed the absorption cross section by the Ar and the Xe targets using (A3) at  $P_{\text{lab}}$  corresponding to the pseudorapidities  $\eta$  of their measurements. We use  $r = 1.31$  fm and  $\lambda$  interpolated from the values in Fig. 6. The results, in mb, are shown in Fig. 7.

We note that  $\sigma$  increases with  $\eta$  to reach a maximum at  $\eta \approx 1.5$  corresponding to the  $\pi^- A$  reaction at  $P_{\text{lab}} \approx 0.290$  GeV/c the well-known  $\Delta(1238)$  resonance, then levels off with small jitters reflecting the structure of  $\pi$ -nucleon scattering. This behavior indicates that as far as the nuclear absorption of the  $\eta$  distributions of  $p + A \rightarrow \pi^- + \dots$ , in general, the effect is negligible for  $\eta > 1.25$ .

In order to check the reliability of our parametrization of the generalized CYY formula, Eq. (5), we have investigated the effect of nuclear absorption of  $\pi^-$  by the target in the case of the NA5 data. For this purpose, we have computed the absorption cross section using the optical model at  $\pi^-$  energies corresponding to  $\eta$  bins of the NA5 experiment. The results, cf. Fig. 7, indicate that the

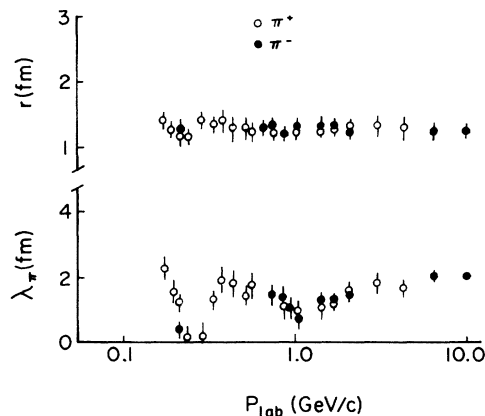


FIG. 6. Optical-model parameters for absorption cross sections of  $\pi^- A$  reactions, Eq. (A3).

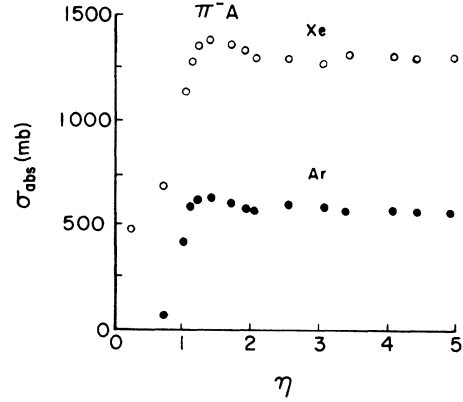


FIG. 7. Nuclear absorption cross section of  $\pi^- A$  as a function of  $\eta = \tanh(P/m)$  according to the optical model, Eq. (A3).

effect is important for the first two bins corresponding to  $\pi^-$  momentum  $\lesssim 107$  MeV/c.

We therefore refit the NA5 data by omitting either one or two first bins around the origin. We find practically the same parameters as before, without cutoff. In Fig. 8 we present the fits with  $1 \leq |\eta| \leq 3$  by the solid curves, the dotted lines being extrapolations outside the fit range. The parameters are

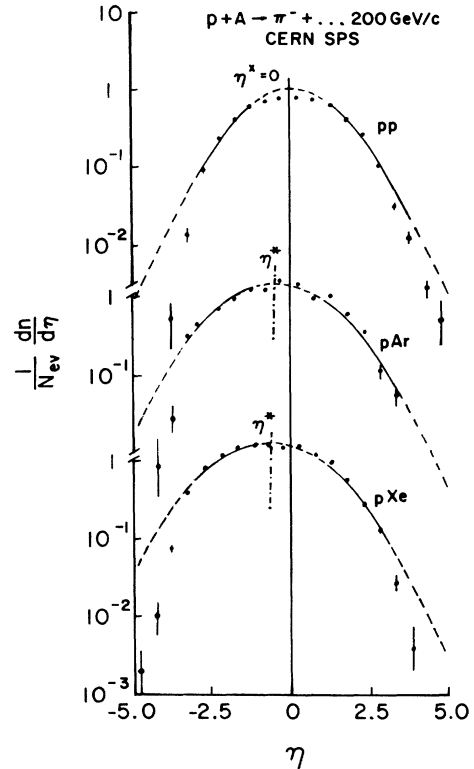


FIG. 8. Same fits as Fig. 1 with  $1.0 < |\eta| < 3.0$  to investigate the effect due to the nuclear absorption of low-energy  $\pi^-$  by the target; the dotted lines are extrapolation, see text.



$$\eta^* = 0.04 \pm 0.01, \quad T_p^* = 0.603 \pm 0.054, \quad N = 42.79 \pm 9.8 \quad \text{for } pp,$$

$$\eta^* = -0.45 \pm 0.5, \quad T_p^* = 0.857 \pm 0.143, \quad N = 62.35 \pm 8.4 \quad \text{for } p\text{Ar},$$

$$\eta^* = -0.68 \pm 0.02, \quad T_p^* = 0.918 \pm 0.097, \quad N = 75.93 \pm 11.0 \quad \text{for } p\text{Xe},$$

comparable to those without cutoff near origin, Table I.

This indicates that no nuclear abruption effect can be detected with the NA5 data. It would be interesting to further investigate the effect of nuclear absorption when other data of high resolution and high statistics will be available.

<sup>1</sup>P. Freier, E. J. Lofgren, E. P. Ney, and F. Openheimer, *Phys. Rev.* **74**, 1818 (1948); A. L. Bradt and B. Peters, *ibid.* **75**, 1779 (1949).

<sup>2</sup>See, e.g., J. D. Bjorken, *Phys. Rev. D* **27**, 140 (1980).

<sup>3</sup>*Quark Matter '87*, proceedings of the Sixth International Conference on Ultrarelativistic Nucleus-Nucleus Collisions, Munster, West Germany, 1987, edited by H. Satz, H. J. Specht, and R. Stock [*Z. Phys. C* **38**, 1 (1988)].

<sup>4</sup>See, e.g., R. Hagedorn, *Riv. Nuovo Cimento* **6**, 1 (1983).

<sup>5</sup>NA5 Collaboration, C. de Marzo *et al.*, (a) *Phys. Rev. D* **26**, 1019 (1982); (b) **29**, 2476 (1984).

<sup>6</sup>N35 Collaboration, (a) H. Ströbele *et al.*, *Z. Phys. C* **38**, 89 (1988); (b) A. Bamberger *et al.*, *Phys. Lett. B* **205**, 583 (1988); (c) *ibid.* **29**, 363 (1984).

<sup>7</sup>WA80 Collaboration, R. Albrecht *et al.*, (a) *Phys. Lett. B* **202**, 596 (1988); (b) *Z. Phys. C* **38**, 97 (1988).

<sup>8</sup>T. F. Hoang, (a) *Z. Phys. C* **45**, 321 (1989); (b) *Phys. Rev. D* **41**, 3520 (1990).

<sup>9</sup>T. T. Chou, Chen Ning Yang, and E. Yen, *Phys. Rev. Lett.* **54**, 510 (1985).

<sup>10</sup>E116 Collaboration, D. S. Barton *et al.*, *Phys. Rev. D* **27**, 2580 (1983). The Al and Ag data are left aside because some of the measurements are missing in their Table II.

<sup>11</sup>Brookhaven National Laboratory Exp. 802, reported by M. J. Tannenbaum, in *Proceedings of the III International Conference on Nucleus-Nucleus Collisions*, St. Mâlo, France, 1988, edited by C. Detraz *et al.* [*Nucl. Phys. A* **488**, 555 (1988)], Fig. 23.

<sup>12</sup>T. F. Hoang, (a) *Phys. Rev. D* **12**, 296 (1975); (b) *ibid.* **38**, 2729 (1988).

<sup>13</sup>E. Fermi, *Phys. Rev.* **81**, 683 (1951).

<sup>14</sup>T. S. Li and K. Young, *Phys. Rev. D* **34**, 142 (1987).

<sup>15</sup>Note that  $T_p^*$  represents the average energy of a secondary  $\pi^-$  in the c.m.s. of the FB's of the projectile and the target [see

Ref. 8(a)],  $T_p^*$  is related to  $T$ :  $T_p^* = 3T + m_\pi$  so that it is practically constant, just like  $T$  as is listed in Tables I and II.

<sup>16</sup>E. R. Nakamura and K. Kudo, *Z. Phys. C* **40**, 81 (1989).

<sup>17</sup>See, e.g., the CERN-SPS experiment of  $p + \text{Ag}$  and  $p + \text{Au}$  at  $P_{\text{lab}} = 360 \text{ GeV}/c$  by the LHS-RCBC Collaboration, J. Bailly *et al.*, *Z. Phys. C* **35**, 301 (1987).

<sup>18</sup>We have used the data in Fig. 23, of Ref. 11.

<sup>19</sup>(a) T. F. Hoang, Bruce Cork, and H. J. Crawford, *Z. Phys. C* **29**, 611 (1985); (b) T. F. Hoang and H. J. Crawford, *ibid.* **43**, 219 (1989).

<sup>20</sup>(a) L. P. Csernai *et al.*, *Phys. Rev. D* **29**, 2669 (1989); (b) S. Daté *et al.*, *ibid.* **32**, 619 (1985).

<sup>21</sup>A. K. Abul-Magd, G. Alberi, and L. Bertocchi, *Phys. Lett.* **30B**, 182 (1969).

<sup>22</sup>We have used the data of the following  $p + A \rightarrow \pi^-$  experiments: (a) 9.9 GeV/c, M.A. Dasaeva *et al.*, *Yad. Fiz.* **39**, 846 (1984) [*Sov. J. Nucl. Phys.* **39**, 536 (1984)]; (b) 28 GeV/c, D. J. Miller *et al.*, *Nuovo Cimento Lett.* **13**, 39 (1976); (c) 360 GeV/c, J. L. Bailly *et al.*, *Z. Phys. C* **40**, 215 (1988). For  $\langle n_- \rangle_{pp}$ , we use the data compiled in Ref. 19(b).

<sup>23</sup>(a) EM07 Collaboration, H. von Gerstoff *et al.*, *Phys. Rev. C* **39**, 1385 (1989); (b) EM01 Collaboration, M. I. Admavich *et al.*, *Phys. Rev. Lett.* **62**, 2801 (1989).

<sup>24</sup>T. F. Hoang, Bruce Cork, and H. J. Crawford, *Z. Phys. C* **29**, 611 (1985).

<sup>25</sup>I. Nevon *et al.*, *Phys. Rev. Lett.* **42**, 1465 (1979); J. W. Cronin *et al.*, *Phys. Rev.* **126**, 259 (1962); M. Longo *et al.*, *ibid.* **125**, 701 (1962); B. W. Allardya *et al.*, *Nucl. Phys. A* **207**, 1 (1973); A. S. Carrol *et al.*, *Phys. Rev. C* **19**, 635 (1976).

<sup>26</sup>G. Höhler *et al.*, *Z. Phys.* **180**, 430 (1964).

<sup>27</sup>An analysis of the NA5 data in terms of the multicollision model has been made by K. Werner, *Phys. Rev. D* **39**, 780 (1989).